Stability of ferromagnetism in the half-metallic pnictides and similar compounds: a first-principles study

E Şaşıoğlu[1], **I Galanakis**[2], **L M Sandratskii**[1] **and P Bruno**[1]

[1] Max-Planck Institut für Mikrostrukturphysik, D-06120 Halle, Germany
[2] Institut of Microelectronics, NCSR 'Demokritos', 15310 Aghia Paraskevi, Athens, Greece

E-mail: ersoy@mpi-halle.de, i.galanakis@fz-juelich.de, lsandr@mpi-halle.de and bruno@mpi-halle.de

Abstract

Based on first-principles electron structure calculations and employing the frozen-magnon approximation, we study the exchange interactions in a series of transition-metal binary alloys crystallizing in the zinc-blende structure and calculate the Curie temperature within both the mean-field approximation and random-phase approximation. We study two Cr compounds, CrAs and CrSe, and four Mn compounds, MnSi, MnGe, MnAs and MnC. MnC, MnSi and MnGe are isovalent to CrAs and MnAs is isoelectronic to CrSe. Ferromagnetism is particular stable for CrAs, MnSi and MnGe: all three compounds show Curie temperatures around 1000 K. On the other hand, CrSe and MnAs show a tendency to antiferromagnetism when compressing the lattice. In MnC the half-metallic gap is located in the majority-spin channel, in contrast to the other five compounds. The large half-metallic gaps, very high Curie temperatures, the stability of the ferromagnetism with respect to the variation of the lattice parameter and a coherent growth on semiconductors make MnSi and CrAs the most promising candidates for use in spintronics devices.

1. Introduction

The emerging field of spintronics [1, 2], also known as magneto- or spin-electronics, has provided a strong motivation towards the fabrication of novel magnetic materials. A strong interest has been focused on the so-called half-metallic ferromagnets, i.e. metallic compounds for which either the majority or minority spin-channel presents a gap at the Fermi level E_F [3]. Such behaviour is detected in various perovskite structures [4], some oxides like CrO_2 [5] and magnetite (Fe_3O_4) [6], several Heusler alloys [7–9], or some diluted magnetic semiconductors [10, 11].

In 2000, Akinaga and collaborators succeeded in growing a thin film of the binary alloy CrAs on top of GaAs [12]. It was found that the CrAs was actually continuing the zinc-blende (zb) structure of GaAs crystallizing in a metastable phase. The most astonishing property was the total spin magnetic moment of 3 μ_B, which is consistent with the half-metallic character predicted by relevant electronic structure calculations published in the same paper and reproduced with larger accuracy in later publications [13, 14]. The thin films of CrAs also have the great advantage of a high Curie temperature T_C, exceeding 400 K (the limit of the magnetometer used in the experiment) [15]. This discovery intrigued the interest of experimentalists and several attempts were made to grow similar metallic compounds as thin films. Zhao *et al* have grown zb CrSb films by molecular beam epitaxy and found a T_C similar to the CrAs case [16]. Moreover, the growth of small zb MnAs islands on GaAs substrates [17] has been achieved and CrAs/GaAs multilayers have been fabricated [18], showing that coherent heterostructures are possible. These half-metallic materials combine high values of T_C with the coherent growth on top of semiconductors, and as the amount of information on the growth increases, they can be considered as very promising candidates for spintronics applications.

Several theoretical studies have been devoted to the zinc-blende compounds of transition elements with group V and VI elements (respectively, pnictides and chalcogenides). The calculations of the total energy and structural optimization show, in agreement with experiment, that the ground state crystal structure of these compounds is not of the zinc-blende type. In most cases the equilibrium crystal structure is of the NiAs type [19]. This structure does not lead to half-metallicity [20–24]. The zinc-blende structure can only be obtained by the epitaxial growth of a few layers on semiconductors. Galanakis and Mavropoulos studied in detail the magnetic properties and the position of the Fermi level in zb V-, Cr- and Mn-pnictides and chalcogenides as a function of the lattice constant [25]. Several authors have confirmed these results [26–32]. Some of the binary semiconductors crystallize in the wurtzite structure and a number of studies have been devoted to such systems [33, 34]. Of special interest is the case of half-metallic zb MnC compound whose properties differ from the properties of other Mn compounds as was shown in [35]. Also the cases of unsupported clusters [36] and nanocrystallites [37] have been studied.

An important aspect of the studies is the stability of the half-metallic gap. It has been shown that the tetragonal deformation of the zb lattice does not destroy the gap [38, 39], and for some systems it even makes the zb structure more stable [40, 41]. In contrast to other half-metallic systems, in the case of the zb transition-metal compounds it is possible to retain the half-metallicity both at the surfaces of these materials [25, 42] and in the case of multilayers with binary semiconductors [43–48]. The V and Cr atoms have the ability to increase their spin moment considerably as a result of decreasing the number of neighbours, keeping in this way the half-metallicity of the system.

In contrast to Cr and V, the Mn spin moment is saturated in these compounds, which leads to the loss of the half-metallicity at the surface [25]. The spin–orbit coupling has a very weak effect on the spin-polarization of the electron states at the Fermi level for the sp atoms up to fifth period of Mendeleev's table [49]. In the case of MnBi, where Bi is a heavy element from the sixth period, the spin–orbit coupling leads to a decrease of the spin-polarization from 100% to 77% [49]. Recently, Chioncel and collaborators studied the influence of the correlation effects on the electron structure of CrAs [50]. They found that the spin–magnon interaction leads to the appearance of non-quasiparticle states in the spin-minority channel. These states are shown to lie above the Fermi level and to be sensitive to the lattice constant.

In contrast to the gap properties, the exchange interactions in these compounds have attracted much less attention. Shirai has shown that in the case of pnictides (VAs, CrAs and MnAs) the ferromagnetic state is energetically preferable compared to the antiferromagnetic

state [13]. Only in the case of zb FeAs was an opposite trend found [13]. Sakuma demonstrated that the Mn compounds isoelectronic to CrAs (MnSi, MnGe and MnSn) are half-metallic ferromagnets [51]. In these compounds, similarly to CrAs, the long-range ferromagnetism is stabilized by the short-range direct Mn–Mn interaction and an indirect interaction through the sp atoms. The Curie temperature in both CrAs and the isoelectronic MnZ compounds was found to exceed 1000 K [51]. Kübler calculated T_C for VAs, CrAs and MnAs and found the largest value of 1041 K in the case of CrAs, compared with 764 K in VAs and 671 K in MnAs [52]. Taking MnAs as an example, it was shown that the loss of the half-metallicity in a compressed lattice leads to a strong decrease of the Curie temperature [52]. Sanyal and collaborators have calculated T_C for V-, Cr- and MnAs compounds assuming the GaAs and InAs lattice constants [28]. Their mean field approximation (MFA) results agree with the calculations of other authors, while the values of T_C obtained with Monte Carlo simulations are ∼100 K lower than the MFA values for VAs and MnAs and ∼300 K lower for CrAs. Note that the mean-field formula for the Curie temperature used in [28, 51] is derived for a single-sublattice system. Therefore the exchange interaction between 3d and sp atoms is not treated. Also the formula of Kübler [52] is derived for a one-sublattice case. In general, the treatment of multiple-sublattice materials requires solving a system of equations with the number of equations equal to the number of sublattices (see section 2). Below, we show that for the materials studied in this paper the one-sublattice approximation is well founded. In other systems, however, it leads to a large error [56, 57].

In this work we report on the theoretical investigation of the magnetic exchange interactions for selected zb compounds. We study two Cr compounds, CrAs and CrSe, and four Mn compounds, MnAs, MnSi, MnGe and MnC. MnAs is isoelectronic to CrSe, whereas the other three Mn compounds are isoelectronic to CrAs. We use the calculated exchange parameters to estimate the Curie temperature in both the mean field approximation (MFA) (T_C^{MFA}) and random phase approximation (RPA) (T_C^{RPA}). Special attention is paid to the influence of the position of the Fermi level on the magnetic properties.

The paper is organized as follows. In section 2, we discuss the calculational technique. In sections 3 and 4, we present the results for the Cr- and Mn-based half-metallic compounds. Section 5 is devoted to MnC. Finally we summarize in section 6.

2. Calculational method

The calculations are carried out using the augmented spherical waves method (ASW) [53] within the atomic-sphere approximation (ASA) [54]. The exchange–correlation potential is chosen in the generalized gradient approximation [55]. A dense Brillouin zone sampling $30 \times 30 \times 30$ is used. The radii of all atomic spheres are chosen equal.

The method of the calculation of the exchange constants has already been presented elsewhere [56] and it was shown to give accurate results for Heusler alloys which have similar structure to the compounds studied here. Here, to make the paper reasonably self-contained, a brief overview is given. We describe the interatomic exchange interactions in terms of the classical Heisenberg Hamiltonian

$$H_{\text{eff}} = -\sum_{\mu,\nu} \sum_{\substack{\mathbf{R},\mathbf{R}' \\ (\mu\mathbf{R}\neq\nu\mathbf{R}')}} J_{\mathbf{R}\mathbf{R}'}^{\mu\nu} \mathbf{s}_{\mathbf{R}}^{\mu} \mathbf{s}_{\mathbf{R}'}^{\nu}. \tag{1}$$

In equation (1), the indices μ and ν number different sublattices, $\mathbf{R}$ and $\mathbf{R}'$ are the lattice vectors specifying the atoms within sublattices, and $\mathbf{s}_{\mathbf{R}}^{\mu}$ is the unit vector pointing in the direction of the magnetic moment at site $(\mu, \mathbf{R})$.

We employ the frozen-magnon approach [58] to calculate interatomic Heisenberg exchange parameters. The calculations involve a few steps. In the first step, the exchange parameters between the atoms of a given sublattice μ are computed. The calculation is based on the evaluation of the energy of the frozen-magnon configurations defined by the following atomic polar and azimuthal angles:

$$\theta_{\mathbf{R}}^{\mu} = \theta, \qquad \phi_{\mathbf{R}}^{\mu} = \mathbf{q} \cdot \mathbf{R} + \phi^{\mu}. \tag{2}$$

The constant phase ϕ^{μ} is always chosen equal to zero. The magnetic moments of all other sublattices are kept parallel to the z axis. Within the Heisenberg model (1) the energy of such configuration takes the form

$$E^{\mu\mu}(\theta, \mathbf{q}) = E_0^{\mu\mu}(\theta) + \sin^2 \theta J^{\mu\mu}(\mathbf{q}) \tag{3}$$

where $E_0^{\mu\mu}$ does not depend on $\mathbf{q}$ and the Fourier transform $J^{\mu\nu}(\mathbf{q})$ is defined by

$$J^{\mu\nu}(\mathbf{q}) = \sum_{\mathbf{R}} J_{0\mathbf{R}}^{\mu\nu} \exp(\mathrm{i}\mathbf{q} \cdot \mathbf{R}). \tag{4}$$

In the case of $\nu = \mu$ the sum in equation (4) does not include $\mathbf{R} = 0$. Calculating $E^{\mu\mu}(\theta, \mathbf{q})$ for a regular $\mathbf{q}$-mesh in the Brillouin zone of the crystal and performing back Fourier transformation, one gets exchange parameters $J_{0\mathbf{R}}^{\mu\mu}$ for sublattice μ. The determination of the exchange interactions between the atoms of two different sublattices μ and ν is discussed in [56].

First, the Curie temperature is estimated within the mean-field approximation (MFA) for the case of a multi-sublattice material by solving the system of coupled equations [56, 59]

$$\langle s^{\mu} \rangle = \frac{2}{3k_{\mathrm{B}}T} \sum_{\nu} J_0^{\mu\nu} \langle s^{\nu} \rangle \tag{5}$$

where $\langle s^{\nu} \rangle$ is the average z component of $\mathbf{s}_{\mathbf{R}}^{\nu}$ and $J_0^{\mu\nu} \equiv \sum_{\mathbf{R}} J_{0\mathbf{R}}^{\mu\nu}$. Equation (5) can be represented in the form of an eigenvalue matrix problem:

$$(\Theta - T\mathbf{I})\mathbf{S} = 0 \tag{6}$$

where $\Theta_{\mu\nu} = \frac{2}{3k_{\mathrm{B}}} J_0^{\mu\nu}$, $\mathbf{I}$ is a unit matrix and $\mathbf{S}$ is the vector of $\langle s^{\nu} \rangle$. The largest eigenvalue of matrix Θ gives the value of $T_{\mathrm{C}}^{\mathrm{MFA}}$ [59].

Within the random phase approximation (RPA) the Curie temperature is given by the relation [60]

$$\frac{1}{k_{\mathrm{B}} T_{\mathrm{C}}^{\mathrm{RPA}}} = \frac{6\mu_{\mathrm{B}}}{M} \frac{1}{N} \sum_{q} \frac{1}{\omega(\mathbf{q})}, \tag{7}$$

where $\omega(\mathbf{q})$ is the spin-wave dispersion. Equation (7) does not take into account the presence of several sublattices and will be used to estimate the Curie temperature with account for the interactions within the sublattice of the 3d atoms. As we will show, these interactions give a leading contribution to the Curie temperature.

3. Cr compounds: CrAs and CrSe

We begin with the discussion of the Cr compounds: pnictide CrAs and chalcogenide CrSe. The half-metallicity in these compounds results from the formation of bonding and antibonding hybrids between the t_{2g} states (d_{xy}, d_{yz}, and d_{xz}) of the transition metal atom (here Cr) and the p states of the four neighbouring sp atoms (As or Se). The hybridizational gap is partly filled by the e_g states of the 3d atom (d_{z^2} and $d_{x^2-y^2}$). The hybridization takes place in both spin channels. The position of the hybridization gap is different for majority and minority electrons
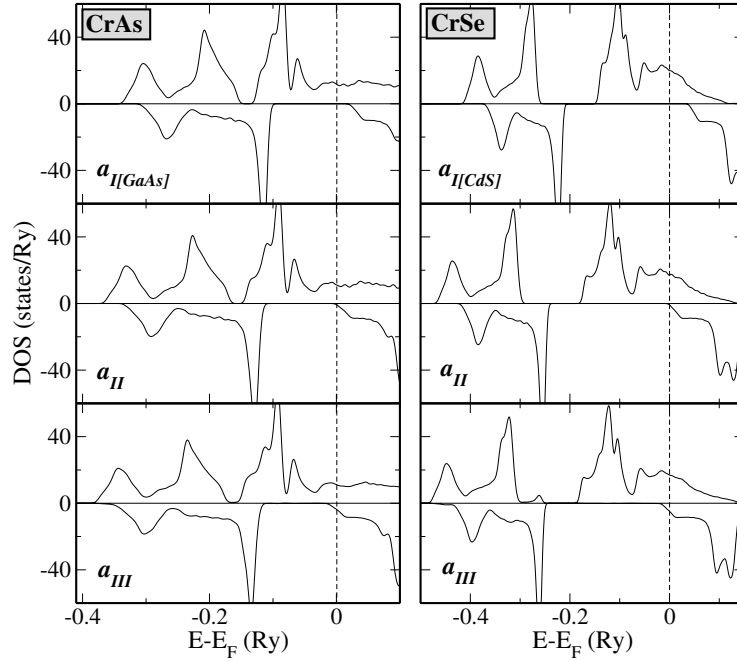
Figure 1. Calculated spin-resolved density of states of CrAs and CrSe. The upper panel corresponds to the experimental lattice constant of GaAs and CdS, respectively, the middle panel to the a_{II} case in table 1 (Fermi level at the higher-energy edge of the half-metallic gap) and the bottom to the a_{III} case in the same table (1% contraction of the lattice constant with respect to the a_{II} case).

as a consequence of the exchange splitting [25]. There are in total four occupied minority states, one coming from the s states of the sp atom and the other three being bonding 3d states. The minority-spin e_g orbitals lie above the Fermi level. Thus the total spin moment M_t in μ_B is given by the relation $M_t = (Z_{tot} - 8)\,\mu_B$, where Z_{tot} is the total number of valence electrons in the unit cell [25]. In the cases of CrAs (11 valence electrons) and CrSe (12 valence electrons) the total spin moment should be 3 and 4 μ_B, respectively.

In table 1 we present the atom-resolved and total spin moments. Notations Void1 and Void2 are used for two types of empty spheres used in our ASA calculations to describe correctly the charge distribution in the zinc-blende structure. For each system we performed calculations for three different lattice parameters. The first parameter (case I) corresponds to the experimental lattice constant of GaAs(CdS) for CrAs(CrSe). For these lattice constants both compounds are half-metals. This is seen in figure 1, where the spin-projected density of states (DOS) is presented. The total spin moment is exactly integer, as expected for a half-metallic system. The Cr atoms possess a very large spin moment of 3.24 μ_B in CrAs that reaches the value of 3.92 μ_B in CrSe. The larger moment of CrSe is a consequence of one extra valence electron per formula unit. Both As and Se atoms have small induced moments antiparallel to the Cr moments. A discussion of the spin moments of the sp atoms and their relative magnitude can be found in [25].

The half-metallic gap of CrSe is much larger than for CrAs. This is explained by the larger Cr moment in CrSe that leads to a larger exchange splitting ΔE_x and, as a result, to a higher position of the minority e_g bands.

In the next step, we compress the lattice simulating a hydrostatic pressure. The contraction of the lattice constant results in a higher energy position of the majority p states with a
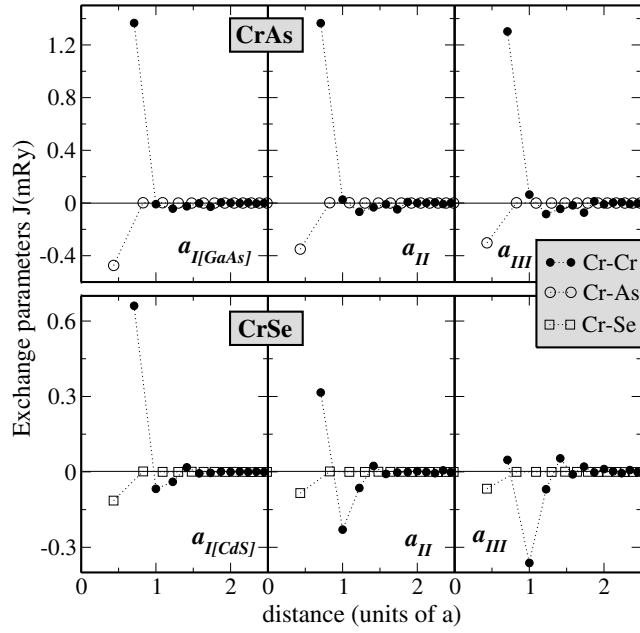
Figure 2. The exchange constants of CrAs (upper panels) and CrSe (lower panels) for three different lattice constants. The left panel corresponds to the experimental lattice constant of GaAs and CdS respectively for CrAs and CrSe, the middle one to case II and the right one to case III.

Table 1. Calculated atom-resolved and total spin moments in μ_B for CrAs and CrSe (second to sixth columns). CrAs and CrSe are half-metallic for the GaAs and CdS experimental lattice constants, respectively. a_{II} means that the Fermi level is at the upper edge of the gap and a_{III} corresponds to 1% contraction with respect to a_{II}.

Compound	a (Å)	m^{Cr}	$m^{As,Se}$	m^{Void1}	m^{Void2}	m^{Total}
CrAs—$a_{I[GaAs]}$	5.65	3.24	−0.31	−0.03	0.10	3.00
CrAs—a_{II}	5.53	3.17	−0.25	−0.03	0.11	3.00
CrAs—a_{III}	5.47	3.10	−0.23	−0.03	0.10	2.95
CrSe—$a_{I[CdS]}$	5.82	3.92	−0.10	0.02	0.16	4.00
CrSe—a_{II}	5.62	3.84	−0.04	0.02	0.18	4.00
CrSe—a_{III}	5.56	3.77	−0.04	0.02	0.16	3.92

corresponding increase of the Fermi energy, E_F. The calculations are performed for two decreased values of the lattice parameter. The first (case II) corresponds to the position of the Fermi level at the bottom edge of the minority-spin conduction band (figure 1). The second parameter (case III) is obtained by a further 1% decrease of the lattice constant. In the latter case the Fermi level lies within the spin-minority conduction band. Since half-metallicity is lost, the total magnetic moment in case III becomes non-integer (see table 1).

The contraction of the lattice leads to an increase of the hybridization between the Cr states and the states of the sp atoms. As the result, both the Cr moment and the induced moment of the sp atom decrease. In case II, the changes of different moments compensate, resulting in the same integer total moment. The decrease of the Cr spin moment causes a small decrease of the width of the gap.

Next we used the frozen-magnon approach to calculate the exchange parameters for both systems and three values of the lattice constants (figure 2). The exchange interaction between

Table 2. Calculated Curie temperatures for CrAs and CrSe. In the third and fourth columns the MFA estimations of T_C^{MFA} are presented, with only the Cr–Cr interactions and with both the Cr–Cr and Cr–As(Se) interactions taken into account, respectively. In the fifth column, the RPA estimation of T_C is presented. Negative values of T_C reveal the instability of the ferromagnetic structure.

Compound	a (Å)	T_C^{MFA} (Cr–Cr)	T_C^{MFA}	T_C^{RPA}
CrAs—$a_{I[GaAs]}$	5.65	1576	1600	1176
CrAs—a_{II}	5.53	1498	1512	1011
CrAs— a_{III}	5.47	1376	1387	860
CrSe— $a_{I[CdS]}$	5.82	706	709	508
CrSe—a_{II}	5.62	109	117	24
CrSe— a_{III}	5.56	−248	−251	−194

the induced moments of the sp atoms is very small and the corresponding parameters are not presented.

For the semiconductor lattice parameter (left panels in figure 2) the interactions are characterized by the large ferromagnetic coupling of the nearest Cr atoms. In CrAs, this coupling is about twice the coupling in CrSe. In the zinc-blende structure the nearest surrounding of a Cr atom is formed by four sp atoms. The second-nearest coordination sphere contains Cr atoms. Although the Cr–sp atom exchange interaction is antiferromagnetic, it makes the parallel directions of the Cr moments energetically preferable. Therefore the indirect exchange interaction of the Cr moments through the sp atoms stabilizes further the ferromagnetic configuration of the Cr moments (a similar situation was found in full-Heusler alloys [61]). The interaction is short range and involves only the nearest Cr atoms.

The influence of the lattice compression is very different for the two systems. In CrAs, the compression leads to a small decrease of the exchange constants revealing the robustness of the ferromagnetism of the compound. On the other hand, in CrSe the effect of the compression is very strong. Already for the a_{II} case where the system is still half-metallic the exchange interaction between the nearest Cr atoms is halved with respect to the case of the CdS lattice constant. The interaction between second-nearest Cr atoms strongly increases, keeping antiferromagnetic character. This is reflected in a very small calculated Curie temperature (see table 2). When the lattice is further compressed and the Fermi level moves into the minority-spin conduction band, the ferromagnetic interaction between the nearest Cr atoms almost vanishes, whereas the antiferromagnetic interaction between the second-nearest Cr atoms increases further. This leads to the instability of the ferromagnetic state.

The calculated Curie temperatures are collected in table 2. They reflect the properties of the exchange interactions discussed above. We report two estimations of the Curie temperature within the MFA, one with only the Cr–Cr interactions taken into account and the other with both Cr–Cr and Cr–sp atom interactions considered, and one RPA estimation.

In case I, for both systems the Curie temperature is much higher than room temperature. For CrAs, T_C is about twice as large as in CrSe, and exceeds 1000 K. The compression of the lattice leads in the case of CrAs to a very moderate decrease of the Curie temperature. In CrSe, T_C drops strongly with decreasing lattice parameter, becoming negative in case III, revealing the instability of the ferromagnetism.

The two mean-field estimations give very similar results (see table 2), revealing the leading role of the Cr–Cr interactions. Therefore the neglect of the inter-sublattice Cr–sp atom interactions does not result in a substantial error for these compounds.

Since the intra-sublattice interactions dominate, the use of the RPA formula (7) is justified. Overall the T_C values within the RPA are by 20–30% smaller than the MFA ones. The difference

Table 3. The equivalent of table 1 for the Mn-based compounds.

Compound	a (Å)	m^{Mn}	m^Z	m^{Void1}	m^{Void2}	m^{Total}
MnAs—$a_{I[InP]}$	5.87	4.16	−0.26	−0.01	0.10	4.00
MnAs—a_{II}	5.73	4.09	−0.20	−0.01	0.11	4.00
MnAs—a_{III}	5.68	4.01	−0.19	−0.01	0.10	3.91
MnGe—$a_{I[GaAs]}$	5.65	3.43	−0.39	−0.08	0.04	3.00
MnGe—a_{II}	5.61	3.40	−0.37	−0.07	0.04	3.00
MnGe—a_{III}	5.55	3.35	−0.34	−0.07	0.04	2.98
MnSi—$a_{I[GaAs]}$	5.65	3.51	−0.49	−0.07	0.05	3.00
MnSi—a_{II}	5.52	3.42	−0.42	−0.06	0.06	3.00
MnSi—a_{III}	5.46	3.37	−0.39	−0.06	0.05	2.97

between MFA and RPA estimations is explained by a different weighting of the spin-wave excitations. In the MFA all excitations are taken with equal weight whereas in the RPA the weight decreases with increasing energy of the excitation [62, 63].

The RPA is expected to provide a better estimation of the Curie temperature. In section 5, we will discuss the relation between the MFA and RPA values of T_C in more detail. The only experimental information about the magnetic transition temperature of the systems considered is that the Curie temperature of CrAs is well above 400 K [12], which is in good correlation with our estimations.

In the case of CrAs we can compare the calculated T_C values of 1600 K within the MFA and 1176 K within the RPA with the results of previous *ab initio* studies. Sanyal and collaborators calculated the Curie temperature within the MFA and found a value of 1320 K for the GaAs experimental lattice constant and 1100 K for the InAs experimental lattice constant [28]. Their Monte Carlo simulations gave for the same lattice constants 980 and 790 K, respectively. Kübler used a Ginzburg–Landau approach with a simplified form of the dynamical susceptibility and a relaxation parameter fitted to reproduce the experimental Curie temperature of NiMnSb. His estimation of T_C of CrAs gives 1041 K [52]. Finally, Sakuma's mean-field calculation for the theoretical equilibrium lattice constant of 5.82 Å gave T_C about 1400 K [51]. Summarizing, all calculations agree that the Curie temperature of CrAs should exceed or be about 1000 K. A high T_C value that is stable with respect to the variation of the lattice constant makes CrAs an interesting candidate for spintronics applications.

4. Mn compounds: MnSi, MnGe and MnAs

We proceed with the discussion of Mn compounds. Here we study MnSi and MnGe, which are isoelectronic to CrAs, and MnAs, which is isoelectronic to CrSe.

In table 3 we present the atom-resolved and total magnetic moments. MnAs with the lattice constant of InP, and MnSi and MnGe with the lattice constant of GaAs, are half-metallic and their total spin moments following the relation presented above are 4 μ_B for MnAs and 3 μ_B for MnSi and MnGe (see table 3 and figure 3). The Mn spin moment is about 3.5 μ_B for MnSi and MnGe, and exceeds 4 μ_B in the case of MnAs, reflecting the presence of one more valence electron in the latter compound. The moments of the sp atoms are antiferromagnetically coupled to the Mn moments. The value of the half-metallic gap is determined by the value of the exchange splitting and the energy position of the p states of the sp atom, while the value of the exchange splitting is governed by the value of the Mn moment. As a result, the largest gap is obtained for MnAs followed by MnSi, and the smallest gap is obtained for MnGe.
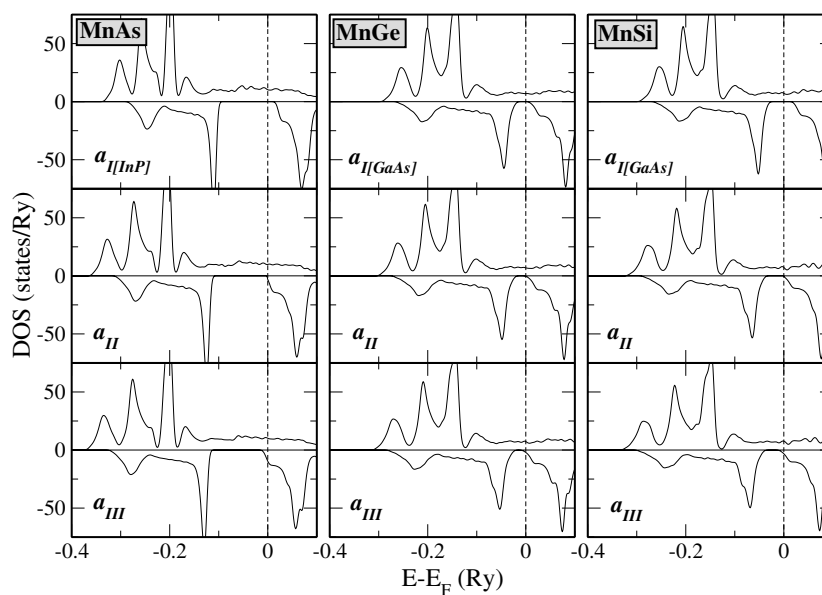
Figure 3. The density of states of MnAs, MnGe and MnSi. See the caption in figure 1 for the description of details.

As for the Cr compounds, the contraction of the lattice increases the energy of the majority p states, leading to an increased Fermi level. For all three compounds the hybridization between the p states of the sp atom and the t_{2g} states of Mn increases and the Mn spin moment slightly decreases with the lattice contraction. The smaller Mn moments and, as a result, smaller exchange splittings lead to slightly smaller gap-widths.

In figure 4 we present the calculated exchange constants. The exchange interaction between the induced moments of sp atoms is very weak and is not presented. There is strong similarity in the behaviour of the exchange parameters for the Mn compounds considered here and the Cr compounds discussed in the preceding section. The properties of MnGe and MnSi are analogous to the properties of the isovalent CrAs, while the properties of MnAs are similar to the properties of isovalent CrSe. Therefore the corresponding parts of the discussion of the Cr compounds remain valid also for the Mn systems.

Ferromagnetism is stabilized by both the direct Mn–Mn exchange interaction and by the indirect interaction through the sp atoms. The exchange interactions are short range and the Mn–Mn exchange constants for MnAs are about a factor two smaller than for MnSi and MnGe.

The compression has little effect on MnSi and MnGe, in contrast to MnAs. Again there is a strong similarity between MnAs and CrSe, although the dependence of the exchange parameters on the lattice constant in MnAs is somewhat weaker. In particular, the antiferromagnetic exchange interaction between second-nearest Mn atoms developing with contraction has a lower value than in CrSe. This results in preserving the ferromagnetic ground state of MnAs for all lattice parameters considered, while in CrSe the ferromagnetic state becomes unstable (see table 2).

The Curie temperatures of the Mn compounds are collected in table 4. Again, as for Cr compounds, the Mn–Mn interaction is dominant and taking into account also the Mn–sp atom exchange interaction influences the value of the Curie temperature weakly. In agreement with the properties of the exchange constants, the Curie temperatures of MnGe and MnSi depend
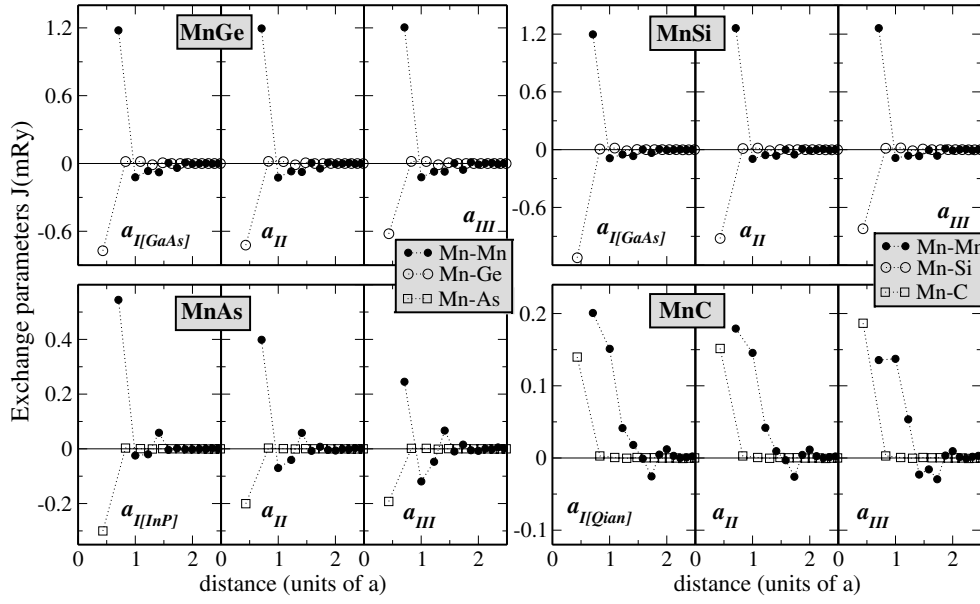
Figure 4. Variation of the exchange constants for the Mn-based compounds. The left panels correspond to the experimental lattice constants of semiconductors (see table 3), middle panels to case II and the right panels to case III.

Table 4. Calculated Curie temperatures for MnAs, MnGe and MnSi. See the caption in table 2 for the description.

Compound	a (Å)	T_C^{MFA}(Mn–Mn)	T_C^{MFA}	T_C^{RPA}
MnAs—$a_{I[InP]}$	5.87	679	701	551
MnAs—a_{II}	5.73	400	417	275
MnAs—a_{III}	5.68	201	230	136
MnGe—$a_{I[GaAs]}$	5.65	1160	1234	716
MnGe—a_{II}	5.61	1180	1241	740
MnGe—a_{III}	5.55	1184	1231	695
MnSi—$a_{I[GaAs]}$	5.65	1255	1402	848
MnSi—a_{II}	5.52	1310	1401	857
MnSi—a_{III}	5.46	1291	1367	911

weakly on the lattice parameter, in contrast to MnAs, where this dependence is strong. The Curie temperature of MnAs at the highest contraction considered assumes a value of about $\frac{1}{4}$th of the Curie temperature at the semiconductor lattice constant. The RPA gives values of T_C that are about 30% smaller than the corresponding values within the MFA. For MnSi and MnGe, the RPA value of T_C also remains considerably above room temperature at all lattice constants studied. The stability of the high T_C value with respect to the variation of the lattice constant makes MnGe and MnSi promising candidates for spintronics applications. MnSi has an additional advantage of a larger half-metallic gap.

Next we compare the results of our calculation of T_C with the results of previous calculations where available. For MnAs, we can compare our MFA estimation of 701 K and RPA estimation of 551 K obtained for the InP lattice constant with the Curie temperatures reported by Sanyal *et al* [28]. The MFA estimation of Sanyal *et al* gave the value of 640 K

Table 5. Calculated spin magnetic moments and Curie temperatures for MnC. The value of 4.20 Å is the equilibrium lattice constant calculated by Qian *et al* [35].

Compound	a (Å)	m^{Mn}	m^Z	m^{Void1}	m^{Void2}	m^{Total}
MnC—$a_{I[35]}$	4.20	1.16	−0.14	−0.01	−0.01	1.00
MnC—a_{II}	4.23	1.16	−0.14	−0.01	−0.01	1.00
MnC—a_{III}	4.27	1.13	−0.16	−0.01	−0.01	1.05

Compound	a (Å)	T_C^{MFA}(Mn–Mn)	T_C^{MFA}	T_C^{RPA}
MnC—$a_{I[35]}$	4.20	520	526	507
MnC—a_{II}	4.23	467	476	458
MnC—a_{III}	4.27	346	363	327

for the InAs lattice parameter, which is very close to the parameter used in our calculations. Their Monte Carlo simulation gave a T_C value of 530 K, which is very close to our RPA estimation. Kübler obtained the value of 671 K for MnAs with the InAs lattice constant. When he compressed the lattice down to the GaAs lattice constant of 5.65 Å, T_C dropped sharply to 210 K [52], in agreement with our results. Finally, Sakuma's MFA estimation of the Curie temperature of MnGe for a lattice constant of 5.82 Å gave a value of about 1200 K, which is very close to our MFA value of 1234 K [51]. Thus the results of different calculations are in reasonable agreement with one another.

5. MnC

The last compound studied in this paper is MnC. This system was predicted to be half-metallic by Qian and collaborators [35]. First we discuss the results of the calculation with the theoretical equilibrium lattice constant reported by Qian *et al*. The magnetic properties of MnC differ from the properties of the Mn compounds discussed above. MnC has 11 valence electrons: 6 majority-spin and 5 minority-spin electrons. This electron distribution results in a magnetic moment which is much smaller than in the compounds discussed above (see table 5). In contrast to the other compounds, the half-metallic gap is now in the majority-spin channel (see figure 5). The majority-spin DOS has the following structure. Low in energy in the interval [−0.55 Ryd, −0.4 Ryd] lie s states. Above, in the interval [−0.4 Ryd, −0.2 Ryd], there are three bonding hybrids between the p states of C and the t_{2g} states of Mn. This is seen in the atom-projected DOS of MnC (right panel in figure 5) where both Mn and C states have similar contribution in this energy interval. The group of states next in energy (the interval [−0.2 Ryd, −0.05 Ryd]) does not hybridize with the lower states. These are the Mn e_g states separated by a gap from the antibonding C p–Mn t_{2g} hybrids. The Fermi level lies within this gap in the majority-spin DOS. For the minority-spin channel, the position of the Fermi level belongs to the region of the e_g states. These states are shifted by the exchange splitting to higher energies with respect to the corresponding majority-spin states.

The comparison of the DOS of half-metallic MnC and MnSi (figure 5) allows us to reveal the reason for the move of the semiconductor-type behaviour from the spin-minority channel in MnSi to the spin-majority channel in MnC. First, the two systems differ by the value of the magnetic moment that leads in the case of MnC to a smaller relative exchange shift of the spin-up and spin-down states and to the occupation of a larger number of the spin-down Mn 3d states. In particular, the minority-spin e_g states are partly occupied in MnC, whereas in MnSi these states lie above the half-metallic gap. Second, there is difference in the position of the e_g states in the hybridizational gap between bonding and antibonding t_{2g}–p hybrids which in the
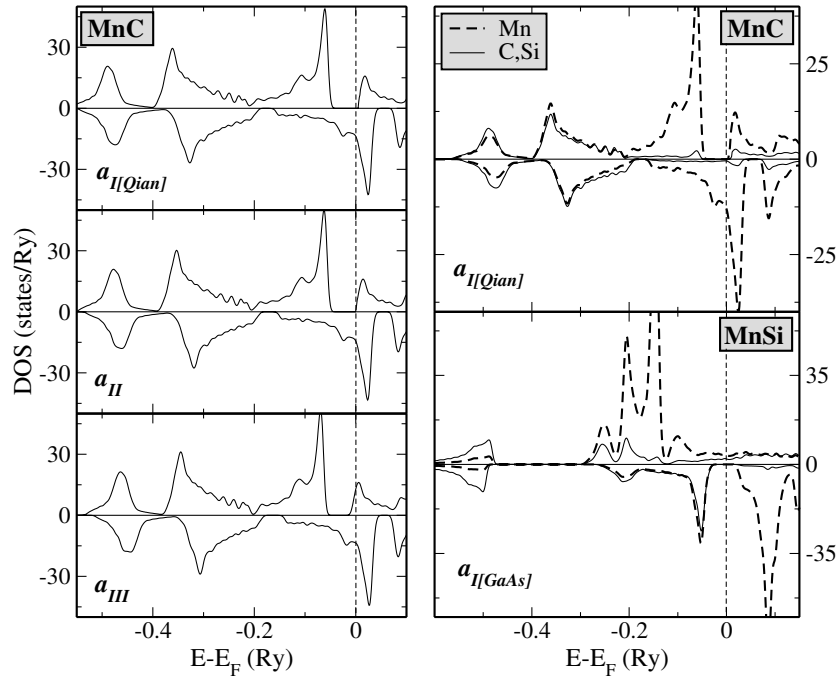
Figure 5. Left panel: calculated spin-resolved DOS of MnC. The upper panel corresponds to the lattice constant given in [35], the middle and lower panels to the a_{II} and a_{III} cases in table 5. Right panel: atom- and spin-resolved DOS for the half-metallic MnC and MnSi compounds.

case of MnSi results in the gap between occupied majority e_g and empty antibonding hybrid states.

To extend the study of MnC to the case where the Fermi level lies at the top-edge of the half-metallic gap (case II) and above it (case III) we need to expand the lattice (see table 5) opposite to all systems considered above where the lattice must be compressed. This difference comes from the move of the semiconductor channel to the majority-spin subsystem. The expansion of the lattice makes the energy bands narrower and decreases the strength of the 3d–p hybridization. At the same time the Mn moment increases, increasing the exchange splitting between majority and minority states. These properties lead to increasing occupation of the majority-spin states and the loss of the half-metallicity (see figure 5).

The calculated exchange constants are presented in figure 4. The ferromagnetism is stabilized by the direct Mn–Mn interactions and the Mn–C ferromagnetic coupling. Since the Mn moment is much smaller than in other compounds the value of the Mn–Mn exchange interaction is substantially lower (see figure 4). On the other hand, in MnC the first- and second-nearest Mn atoms are characterized by a similar strength of the ferromagnetic exchange interaction, while in other systems only the nearest Mn atoms interact strongly. The expansion of the lattice leads to decreasing Mn–Mn exchange interactions.

The calculated Curie temperatures are presented in table 5. The Curie temperature of MnC is smaller than in other Mn compounds, being about 500 K (it is comparable with the RPA estimation of T_C of MnAs). The value of the Curie temperature decreases with expansion of the lattice, showing again that half-metallicity is favorable for high Curie temperature.

A remarkable feature of the calculation for MnC is a very small difference between the T_C values estimated within the MFA and the RPA. In section 3 we briefly discussed the reason
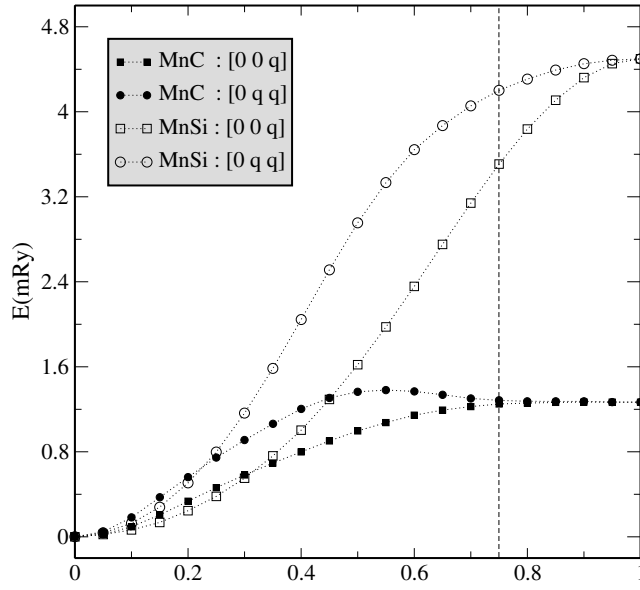
Figure 6. Frozen-magnon energies in MnC and MnSi for [00q] and [0qq] directions in the Brillouin zone. The vertical broken line shows the Brillouin zone boundary for the [0qq] direction.

behind the different values of the Curie temperatures estimated within the MFA and the RPA. A striking contrast between MnC and the systems considered in the previous sections allows for gaining a deeper insight into the physics of the formation of the Curie temperature. We will base our analysis on the comparison of two systems: MnC and MnSi. Characterizing the relative difference of the MFA and RPA values of the Curie temperature by the relation $[T_{\mathrm{C}}^{\mathrm{MFA}} - T_{\mathrm{C}}^{\mathrm{RPA}}]/T_{\mathrm{C}}^{\mathrm{RPA}}$, we get for MnC a small value of 2.5% compared to a large value of 47% in MnSi.

In the MFA, the Curie temperature is determined by an arithmetic average of the magnon energies, while in the RPA T_{C} is determined by the harmonic average of the same quantities. It is an arithmetic property that the MFA estimation is larger than the RPA one or equal to it if all averaged numbers are equal to each other. In terms of magnon energies, $T_{\mathrm{C}}^{\mathrm{MFA}}$ is equal to $T_{\mathrm{C}}^{\mathrm{RPA}}$ in the case that the magnon spectrum is dispersionless: the magnon energy does not depend on the wavevector **q**.

In figure 6 we plot the frozen-magnon energies of MnSi and MnC for two selected directions in reciprocal space. We see that the MnC curves are flat in the second half of the **q** interval, showing here a very weak dispersion. On the other hand, the MnSi curves are much closer to a simple cosinusoidal form with considerable dispersion in this part of the **q** interval. Comparing now the low-**q** parts of the curves we notice that the MnC curves lie higher than the MnSi curves. Therefore, the relative contribution of the low-energy magnons to the RPA value of the Curie temperature is less important in MnC compared to MnSi.

This combination of features of the wavevector dependences of the frozen-magnon energies is responsible for a much smaller difference between the RPA and MFA estimations of the Curie temperature in the two cases. Since the form of the magnon dispersion is reflected in the properties of the interatomic exchange interactions, it is instructive to compare the patterns of the exchange interactions of the two systems. Taking into account that only Mn–Mn interactions contribute importantly in the Curie temperature we will focus on the comparison of these interactions.

The analysis of the Mn–Mn exchange interactions in MnSi and MnC (see figure 4) shows a strong difference between the two systems. In MnSi, only the first-neighbour exchange interaction plays an important role. All other interactions are much smaller. On the other hand, in the case of MnC the second-neighbour interaction is comparable with the first-neighbour one. The further few interactions, though sizable, play a less important role. The presence of two first coordination spheres with similar values of the exchange interactions, on the one hand, makes the exchange interaction in MnC more long ranged and, on the other hand, it effectively increases the coordination number of the atoms with leading exchange interaction. Either of these properties leads to a better accuracy of the MFA estimation.

6. Summary and conclusions

We have presented a detailed study of the stability of the ferromagnetism in six transition-metal compounds crystallizing in the zinc-blende structure. We calculated the electronic structure from first principles and employed the frozen-magnon approximation to evaluate the exchange parameters and the Curie temperature. In the calculation of the Curie temperature we used both the mean-field and random-phase approximations.

Considering the CrAs and CrSe compounds, we found in the case of CrAs a very high Curie temperature, exceeding 1000 K. The ferromagnetism of CrAs is stable with respect to the compression of the lattice. On the other hand, CrSe possesses about a half as big Curie temperature, which decreases strongly with lattice compression.

The properties of MnSi and MnGe are similar to the properties of isovalent CrAs, while the properties of MnAs are similar to the properties of isovalent CrSe.

MnC presents an interesting case that differs from all other systems studied. This system is also half-metallic, with the half-metallic gap in the majority-spin channel, in contrast to other systems, where the half-metallic gap is in the minority-spin subsystem. The Curie temperature of MnC was found to be about 500 K.

In all cases considered we found that half-metallicity is favorable for ferromagnetism and leads to an increased Curie temperature.

We conclude that two compounds, MnSi and CrAs, possess properties which make them promising candidates for spintronics applications: large half-metallic gap and high Curie temperature. The stability of the Curie temperature in these systems allows us to expect that, being grown on the substrate of a binary semiconductor, they will preserve the desired magnetic properties.

Acknowledgment

References

[1] Prinz G A 1998 *Science* **282** 1660
[2] de Boeck J, van Roy W, Das J, Motsnyi V, Liu Z, Lagae L, Boeve H, Dessein K and Borghs G 2002 *Semicond. Sci. Technol.* **17** 342
    de Boeck J, van Roy W, Motsnyi V, Liu Z, Dessein K and Borghs G 2002 *Thin Solid Films* **412** 3
[3] de Groot R A, Mueller F M, van Engen P G and Buschow K H J 1983 *Phys. Rev. Lett.* **50** 2024
[4] Soulen R J Jr, Byers J M, Osofsky M S, Nadgorny B, Ambrose T, Cheng S F, Broussard P R, Tanaka C T, Nowak J, Moodera J S, Barry A and Coey J M D 1998 *Science* **282** 85

[5]   Schwarz K 1986 *J. Phys. F: Met. Phys.* **16** L211
      Korotin M A, Anisimov V I, Khomskii D I and Sawatzky G A 1998 *Phys. Rev. Lett.* **80** 4305
[6]   Yanase A and Siratori K 1984 *J. Phys. Soc. Japan* **53** 312
[7]   Galanakis I, Dederichs P H and Papanikolaou N 2002 *Phys. Rev.* B **66** 134428
[8]   Galanakis I, Dederichs P H and Papanikolaou N 2002 *Phys. Rev.* B **66** 174429
[9]   Galanakis I 2004 *J. Phys.: Condens. Matter* **16** 3089
[10] Akai H 1998 *Phys. Rev. Lett.* **81** 3002
[11] Sandratskii L M and Bruno P 2002 *Phys. Rev.* B **66** 134435
[12] Akinaga H, Manago T and Shirai M 2000 *Japan. J. Appl. Phys.* **39** L1118
[13] Shirai M 2001 *Physica* E **10** 143
[14] Shirai M 2003 *J. Appl. Phys.* **93** 6844
      Shirai M 2004 *J. Phys.: Condens. Matter* **16** S5525
[15] Mizuguchi M, Akinaga H, Manago T, Ono K, Oshima M and Shirai M 2002 *J. Magn. Magn. Mater.* **239** 269
[16] Zhao J H, Matsukura F, Takamura K, Abe E, Chiba D and Ohno H 2001 *Appl. Phys. Lett.* **79** 2776
[17] Ono K, Okabayashi J, Mizuguchi M, Oshima M, Fujimori A and Akinaga H 2002 *J. Appl. Phys.* **91** 8088
[18] Mizuguchi M, Akinaga H, Manago T, Ono K, Oshima M, Shirai M, Yuri M, Lin H J, Hsieh H H and Chen C T
      2002 *J. Appl. Phys.* **91** 7917
[19] Landolt-Börnstein 1988 *New Series* Group IIIa, vol 27, ed K Adachi and S Ogawa (Heidelberg: Springer)
[20] Wei S H and Zunger A 1987 *Phys. Rev.* B **35** 2340
[21] Sanvito S and Hill N A 2000 *Phys. Rev.* B **62** 15553
[22] Continenza A, Picozzi S, Geng W T and Freeman A J 2001 *Phys. Rev.* B **64** 085204
[23] Zhao Y-J, Geng W T, Freeman A J and Delley B 2002 *Phys. Rev.* B **65** 113202
[24] Xie W-H, Xu Y-Q, Liu B G and Pettifor D G 2003 *Phys. Rev. Lett.* **91** 037204
[25] Galanakis I and Mavropoulos Ph 2003 *Phys. Rev.* B **67** 104417
[26] Liu B G 2003 *Phys. Rev.* B **67** 172411
[27] Pask J E, Yang L H, Fong C Y, Pickett W E and Dag S 2003 *Phys. Rev.* B **67** 224420
[28] Sanyal B, Bergqvist L and Eriksson O 2003 *Phys. Rev.* B **68** 054417
[29] Xu Y G, Liu B G and Pettifor D G 2002 *Phys. Rev.* B **66** 184435
[30] Xie W-H and Liu B G 2003 *J. Phys.: Condens. Matter* **15** 5085
[31] Yao K L, Gao G Y, Liu Z L and Zhu L 2005 *Solid State Commun.* **133** 301
[32] Zhang M, Hu H, Liu G, Cui Y, Liu Z, Wang J, Wu G, Zhang X, Yan L, Liu H, Meng F, Qu J and Li Y 2003
      J. Phys.: Condens. Matter **15** 5017
      Zhang M, Hu H, Liu G, Liu Z, Cui Y and Wu G 2004 *J. Low Temp. Phys.* **135** 267
      Zhang M, Hu H, Liu Z, Liu G, Cui Y and Wu G 2004 *J. Magn. Magn. Mater.* **270** 32
[33] Xie W-H, Liu B G and Pettifor D G 2003 *Phys. Rev.* B **68** 134407
[34] Zhang M, Brück E, de Boer F R, Liu G D, Hu H N, Liu Z H, Cui Y T and Wu G C 2004 *J. Mater. Res.* **19** 2738
[35] Qian M C, Fong C Y and Yang L H 2004 *Phys. Rev.* B **70** 052404
[36] Nakao M 2004 *Phys. Rev.* B **69** 214429
[37] Qian M C, Fong C Y, Pickett W E and Wang H Y 2004 *J. Appl. Phys.* **95** 7459
[38] Shi L J and Liu B G 2005 *J. Phys.: Condens. Matter* **17** 1209
[39] Yamana K, Geshi M, Tsukamoto H, Uchida I, Shirai M, Kusakabe K and Suzuki N 2004 *J. Phys.: Condens.
      Matter* **16** S5815
[40] Zhao Y-J and Zunger A 2005 *Phys. Rev.* B **71** 132403
[41] Zheng J-C and Davenport J W 2004 *Phys. Rev.* B **69** 144415
[42] Galanakis I 2002 *Phys. Rev.* B **66** 012406
[43] Fong C Y, Qian M C, Pask J E, Yang L H and Dag S 2004 *Appl. Phys. Lett.* **84** 239
      Fong C Y and Qian M C 2004 *J. Phys.: Condens. Matter* **16** S5669
[44] Mavropoulos Ph, Galanakis I and Dederichs P H 2004 *J. Phys.: Condens. Matter* **16** 4261
[45] Nagao K, Shirai M and Miura Y 2004 *J. Appl. Phys.* **95** 6518
[46] Geshi M, Kusakabe K and Suzuki N 2004 *J. Phys.: Condens. Matter* **16** S5701
[47] Qian M C, Fong C Y, Pickett W E, Pask J E, Yang L H and Dag S 2005 *Phys. Rev.* B **71** 012414
[48] Bengone O, Eriksson O, Fransson J, Turek I, Judrnovsky J and Drchal V 2004 *Phys. Rev.* B **70** 035302
[49] Mavropoulos Ph, Sato K, Zeller R, Dederichs P H, Popescu V and Ebert H 2004 *Phys. Rev.* B **69** 054424
[50] Chioncel L, Katsnelson M I, de Wijs G A, de Groot R A and Lichtenstein A I 2005 *Phys. Rev.* B **71** 085111
[51] Sakuma A 2002 *J. Phys. Soc. Japan* **71** 2534
[52] Kübler J 2003 *Phys. Rev.* B **67** 220403
[53] Williams A R, Kübler J and Gelatt C D 1979 *Phys. Rev.* B **19** 6094

[54] Andersen O K 1975 *Phys. Rev.* B **12** 3060
[55] Perdew J P and Wang Y 1992 *Phys. Rev.* B **45** 13244
[56] Şaşıoğlu E, Sandratskii L M and Bruno P 2004 *Phys. Rev.* B **70** 024427
[57] Şaşıoğlu E, Sandratskii L M and Bruno P 2005 *J. Phys.: Condens. Matter* **17** 995
[58] Rosengaard N M and Johansson B 1997 *Phys. Rev.* B **55** 14975
     Halilov S V, Eschrig H, Perlov A Ya and Oppeneer P M 1998 *Phys. Rev.* B **58** 293
     Sandratskii L M and Bruno P 2003 *Phys. Rev.* B **67** 214402
[59] Anderson P W 1963 Theory of magnetic exchange interactions: exchange in insulators and semiconductors
     Solid State Physics vol 14, ed F Seitz and D Turnbull (New York: Academic) pp 99–214
[60] Şaşıoğlu E, Sandratskii L M and Bruno P 2005 *J. Magn. Magn. Mater.* **290/291** 385
[61] Kübler J, Williams A R and Sommers C B 1983 *Phys. Rev.* B **28** 1745
[62] Pajda M, Kudrnovsky J, Turek I, Drchal V and Bruno P 2001 *Phys. Rev.* B **64** 174402
[63] Bouzerar G, Kudrnovský J, Bergqvist L and Bruno P 2003 *Phys. Rev.* B **68** 081203